CONNECTIVITY-BASED PARCELLATION OF FUNCTIONAL SUB-REGIONS FROM BRAIN FMRI SIGNALS

Nandinee Fariah Haq, Sun Nee Tan, Martin J. McKeown, Z. Jane Wang

The University of British Columbia
Vancouver, Canada.

ABSTRACT

In this paper, we propose a connectivity-based framework to extract functional sub-regions (subROIs) in the putamen from fMRI signals. The proposed framework aims to generate a network that represents the connectivity patterns of the putamen voxels among themselves, and with the other brain regions. A spatial constraint is introduced into the network generation framework to ensure the spatial continuity of the final subROIs. A eigenvalue-based community detection approach is then incorporated to sub-divide the network into two functionally connected and spatially continuous sub-regions. The framework is applied to synthetic datasets to evaluate its performance wih respect to other literature-based approaches. The proposed framework is finally applied to resting state fMRI data from five healthy subjects to parcellate the putamen region into two functional subROIs. Although the framework is developed for putamen, it can generally be applied to other brain region subROI parcellation tasks.

Index Terms— functional MRI, brain connectivity, community detection, putamen

1. INTRODUCTION

The human brain consists of structurally and functionally interconnected regions. Connectivity based parcellation targets to divide these regions-of-interest (ROI) into distinct sub-regions-of-interest (subROIs) based on their differences in the connectivity patterns extracted from brain fMRI signals. One important brain region that is repeatedly reported in the literature to have several functional sub-regions is the striatum of the basal ganglia [1, 2]. Striatum is functionally sub-divided into two subROIs, namely- dorsolateral striatum (DLS) which is associated with habitual control and dorsomedial striatum (DMS) which is associated with goal-oriented control [3]. Parcellation of putative basal ganglia subROIs can play an essential role in developing more detailed models of whole-brain connectivity network [4] and in evaluating hypotheses about healthy aging and development [5, 6]. Moreover, exploration of the connectivity patterns of the functional subROIs inside striatum, specifically putamen and caudate, is believed to be of great importance in understanding degenerative basal ganglia disorders such as Parkinson's disease and Huntington's disease [7, 8].

The functional subROI parcellation studies reported in the literature can be divided into two categories- clustering-based approaches [9, 10, 11, 12], and graph or network-based approaches [7, 13]. Most of the clustering based approaches require rigorous preprocessing and denoising steps to obtain spatially continuous results since they are very sensitive to outliers. On the other hand the graph-based parcellation methods do not impose spatial continuity and therefore in cases where there are outlier voxels owing to head movement and other artifacts, these approaches may not generate spatially continuous subROIs. Recently Zhang *et al.* [14] proposed a parcellation technique that incorporates the spatial information. However, this method does not consider the voxel-connectivities within the ROI and the robustness of the method highly depends on its optimization parameters. Therefore there is still a need for a complete framework for functional subROI parcellation that can incorporate both the inter-ROI and intra-ROI connectivity patterns while imposing spatial continuity for subROIs.

In this paper, we propose a framework to define spatially continuous functional subROIs within a brain region by exploring functional connectivities between themselves and with a few other ROIs. We develop a putamen functional connectivity network by taking into consideration the spatial location and connectivities within putamen, and the connectivities of other brain regions with putamen. A community detection approach is then adapted to extract two functional sub-regions from the connectivity network. The proposed framework imposes spatial continuity on the subROIs which is often ignored in the literature. Moreover while the most literature-based approaches focus on either intra-region connectivity or inter-region connectivity to parcellate the ROIs, the proposed framework considers both and generates a complete representation of the overall connectivity characteristics inside the putamen. Although the framework is developed for putamen parcellation, it is generally applicable to other brain region parcellation problems with similar challenges.

Corresponding authors: N.Haq (nandinee@ece.ubc.ca), Z.J.Wang (zjanew@ece.ubc.ca).

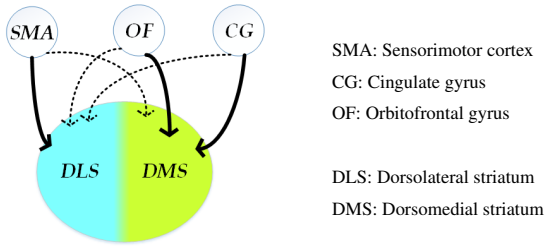

Fig. 1: Illustration of the connectivity patterns of functional subROIs in the putamen region with the reference brain ROIs. The solid lines denote strong connectivity and the dotted lines denote weak connectivity.

2. MATERIALS AND METHODS

In this section, we will describe the datasets used in this work and the proposed framework for separating a given ROI into two or more functionally connected and spatially consistent subROIs. Throughout this paper, the term *task ROI* is used to denote the ROI which we want to divide into subROIs, and *reference ROI* is used to denote other brain ROIs which interact with the task ROI.

2.1. Functional SubROI Parcellation

In this work, we formulated the parcellation of functionally consistent and spatially confined subROIs in putamen as a weighted-graph clustering problem in the voxel space. The putamen region can be divided into two functional subROIs namely DLS and DMS, and these two functional subROIs demonstrates different connectivity patterns with three other brain regions– sensorimotor area (SMA), orbitofrontal gyrus (OF), and cingulate gyrus (CG). SMA has strong connectivity with DLS and weaker connectivity with DMS whereas OF and CG show strong connectivity with DMS and weaker connectivity with DLS [7]. Fig. 1 shows the connectivity pattern of the subROIs with the reference ROIs.

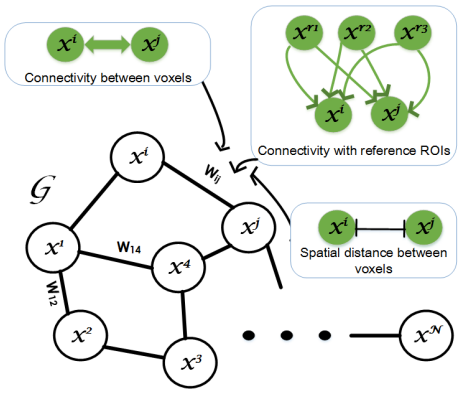

Fig. 2: Illustration of the putamen connectivity network generation.

Functional subROIs in putamen can be extracted from their connectivity patterns among themselves and with three other brain reference regions- SMA, CG and OF. In this work we generated an undirected weighted graph from the connectivity pattern of the putamen voxels, and then clustered the voxels into two spatially continuous subROIs by applying state-of-the-art community detection method. The generation of the network, $\mathcal{G}$ is graphically shown in Fig. 2. To generate the network, each voxel within the putamen region $(x^i, i = 1, 2, .., N)$ is represented by a node and the edge weights between the i^th voxel, x^i and j^th voxel, x^j are derived from the brain connectivity pattern as follows:

$$\mathcal{W}^{ij} = \begin{cases} 0 & \text{for } i = j \\ W^{ij}_{task} \times W^{ij}_{ref} & \text{for } i \neq j \end{cases} \quad (1)$$

Here $\mathcal{W}^{ij}$ is set to zero when $i = j$ to eliminate self-loops in $\mathcal{G}$. The first weight term W_{task} is associated with the the connectivity pattern among the putamen voxels, and is defined as the average connectivity among putamen voxels as a function of their spatial distances, d:

$$W_{task}(d) = \delta^T(d) \times C_{task}(d) \quad (2)$$

where $C^{task}(d)$ denotes the fitted value of the correlation coefficients inside putamen region at a distance d, and $\delta^T(d) = 1$ if $d \leq T$ and zero otherwise. This thresholding ensures that spatially distant voxels do not share edges in the generated network $\mathcal{G}$ and are well separated, ensuring that the final clusters are spatially continuous.

The second weight term, W^{ij}_{ref} in Eqn. 1 is associated with the connectivity pattern of the putamen voxels with the reference brain regions. Ideally, two putamen voxels from the same functional subROI will have similar connectivity to each of the reference ROIs, and the difference between their connectivities with the reference regions will be zero. W^{ij}_{ref} between voxels x^i and x^j is defined as a measure of how close their connectivities are to this ideal behaviour:

$$W^{ij}_{ref} = 1 - \frac{\sum_{m=1}^{M} |C^{m,i}_{ref} - C^{m,j}_{ref}|}{M} \quad (3)$$

Here $C^{m,i}_{ref}$ and $C^{m,j}_{ref}$ are the connectivities between reference ROI m and task ROI voxels x^i and x^j respectively. M is the total number of reference ROIs. The connectivity C_{ref} is defined in terms of partial correlation coefficients between the temporal signals of the task ROI voxels and the average temporal signal of the reference ROI region, controlling for the remaining reference ROIs. The partial correlation coefficient is used here to remove the effect of other reference ROIs while calculating connectivities. Defining the final edge weight as in Eqn. 1 ensures that the three factors are incorporated in the final edge weight. First, W_{ref} ensures the voxels with similar connectivities with the reference ROIs share stronger edges than others. Second, the formulation of W_{task}

ensures the edge weight between voxels are modulated based on their connectivities inside the task ROI (putamen). And finally, W_{task} also ensures that the edge weight decreases exponentially with the distance and goes to zero beyond a certain threshold T so that distant voxels are well-separated or disconnected, hence ensuring that the final clusters are not only functionally connected, but also spatially continuous.

After generating the functional connectivity network, $\mathcal{G}$, we extracted the subROIs from the network's adjacency matrix following the procedure described in [15]. The ratio of the first and second eigenvectors of the adjacency matrix was calculated and k-means algorithm was applied on the ratios to extract the functional subROIs. Detailed description of the network generation and subROI extraction framework can be found in [16].

2.2. Datasets

2.2.1. Synthetic Dataset

Two sets of synthetic dataset is generated in this work to evaluate the performance of the proposed method in different settings. The datasets are generated such that it mimics the real fMRI conditions in putamen. The first synthetic dataset (Dataset-I) is a $10\times10\times10$ cubic volume that is functionally divided into two sub-regions-of-interest (subROIs) - $\mathcal{A}$ and $\mathcal{B}$. To ensure the synthetic dataset is compliant with real fMRI conditions in our problem, three reference regions, x, y and z, are generated and the signals in two sub-ROIs, $i_{\mathcal{A}}$ and $i_{\mathcal{B}}$, are generated such that $\mathcal{A}$ has strong connectivity with x, whereas $\mathcal{B}$ has strong connectivity with y and z. The temporal signals for each of the regions are generated using the following model:

$$\begin{aligned} i_x &= \theta_x m_s + (1-\theta_x) l_s + \epsilon_x \\ i_y &= \theta_y n_s + (1-\theta_y) l_s + \epsilon_y \\ i_z &= \theta_z n_s + (1-\theta_z) l_s + \epsilon_z \\ i_{\mathcal{A}} &= \alpha[\theta_{\mathcal{A}} m_s + (1-\theta_{\mathcal{A}}) l_s] + (1-\alpha) k_s + \epsilon_{\mathcal{A}} \\ i_{\mathcal{B}} &= \beta[\theta_{\mathcal{B}} n_s + (1-\theta_{\mathcal{B}}) l_s] + (1-\beta) r_s + \epsilon_{\mathcal{B}} \\ l_s, m_s, n_s, k_s, r_s &\sim \mathcal{N}(0,1) \\ \epsilon_x, \epsilon_y, \epsilon_z, \epsilon_{\mathcal{A}}, \epsilon_{\mathcal{B}} &\sim \mathcal{N}(0, \sigma_N^2) \\ \theta_x, \theta_y, \theta_z, \theta_{\mathcal{A}}, \theta_{\mathcal{B}}, \alpha, \beta &\sim \mathcal{U}[0.5, 0.9]. \end{aligned} \tag{4}$$

Here i_x, i_y and i_z denote signals in the reference regions x, y and z respectively. The temporal signals are 240-time point long. The subROIs $\mathcal{A}$ and $\mathcal{B}$ consists of 440 and 560 voxels respectively. Fig. 3 shows the synthetic data generation process.

Dataset-I is generated by using a fixed SNR (here SNR = 6 dB) for all the voxels. For Dataset-II, we randomly chose 100 voxels in each of the sub-regions $\mathcal{A}$ and $\mathcal{B}$ and used a lower SNR (here SNR = -10 dB) to generate the signals for those voxels. These 200 voxels serve as the outliers and the rest of the voxels are generated using SNR = 6 dB as Dataset-I. The procedure is repeated 50 times so that Dataset-I and Dataset-II each contains 50 sets of data.

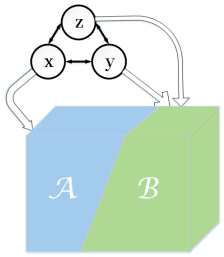

Fig. 3: Illustration of the synthetic data generation process. Here the cubic volume is divided into two functional subROIs– $\mathcal{A}$ and $\mathcal{B}$. x, y and z are three interconnected reference ROIs, where $\mathcal{A}$ is strongly associated with x and $\mathcal{B}$ is strongly associated with y and z.

2.2.2. fMRI Dataset

The fMRI dataset consists of five healthy subjects recruited from the Pacific Parkinson's Research Centre Movement Disorders Clinic at The University of British Columbia. MRI examinations were performed on a Philips 3 T MRI scanner (Achieva, Philips Healthcare, Best, The Netherlands) equipped with a headcoil. The subjects lied on their back with their eyes closed during the examination and whole brain three-dimensional $T1$-weighted images with 170 axial slices were acquired. Each functional run spanned eight minutes during which blood oxygen level dependent (BOLD) contrast echo-planar (EPI) $T2^*$-weighted images were acquired with a repetition time of 1985 ms, echo time of 37 ms and flip angle of 90°. The field of view (FOV) was set to 240 mm which included the cerebellum ventrally as well as the dorsal surface of the brain. In total 240 time-points were acquired with 36 axial slices of 3 mm thickness and 1 mm gap thickness. The matrix size was 128×128 and pixel size was 1.9 mm$\times$1.9 mm. The study was approved by the Clinical Research Ethics Board of the University of British Columbia and the patients had given their informed written consent prior to the study.

The raw fMRI data was pre-processed using the pipeline described in [17] and 54 regions-of-interest (ROI) were extracted using the Freesurfer software [18]. The extracted ROIs were also visually checked by experienced neurologists if needed. All data analysis were done on the unwarped images (in the native space) on a subject-by-subject basis rather than warping images into a common template. In this work, we used four ROIs from the left hemisphere of the brain namely, sensorimotor area (SMA), orbitofrontal gyrus (OF), cingulate gyrus (CG) and the putamen. To form the orbitofrontal gyrus we merged both medial and lateral orbitofrontal cortices, the cingulate gyrus is formed by merging

the anterior and posterior cingulate gyri and the sensorimotor area consists of the primary motor and somatosensory cortex.

3. RESULTS

We applied the proposed framework on two sets of synthetic datasets and compared the parcellation results generated by our proposed framework with three other literature-based functional ROI parcellation methods. To compare the outcomes from different algorithms we calculated the misclassification error defined as the total number of misclassified voxels over the total number of voxels in the task region. Table 1 reports the average misclassification error over 50 sets of data for each of the datasets. The *k*-means clustering is implemented according to [10], the modularity detection algorithm is implemented according to [7] and the spatially regularized regression model is developed according to [14]. For Dataset-I, all methods except the spatially regularized regression method correctly identified the underlying clusters. However, at the presence of outliers in Dataset-II, our proposed method outperformed the *k*-means and modularity detection method and generated comparable performance with the spatially regularized regression method. Note that the spatially regularized regression method generates one parcellation result for each of the three reference ROIs, and out of these three results, in Table 1 we reported the result that best matches with the ground truth. In other cases the spatially regularized method generates a lot of misclassified voxels (error 5-56%), and when the ground truth is not available, it is impossible to determine which parcellation result is accurate out of these three different results .

Table 1: Percentage of errors for synthetic datasets. The dataset generation procedure is repeated 50 times for each of the datasets, and the errors are reported as average error percentage over 50 datasets.

	Dataset-I	**Dataset-II**
Proposed method	**0.00%**	**2.50%**
k-means clustering [10]	0.00%	9.99%
Modularity detection [7]	0.00%	5.97%
Spatially regularized regression [14]	0.86%	1.10%

We then applied the proposed framework in the putamen region to extract two functional subROIs- DLS and DMS. Three reference regions - sensorimotor area, cingulate gyrus, and orbitofrontal gyrus are considered to sub-divide the putamen region into functional subROIs. After clustering the putamen voxels into two groups using the proposed framework, we utilized prior anatomical knowledge about the position of DLS and DMS to label the clusters. Anatomically DLS resides at the lateral part of the striatum whereas DMS lies in the medial portion. We calculated the spatial location of the centroids of the generated clusters. The cluster with the laterally positioned centroid is then labelled as DLS and the other cluster is labelled as DMS. Fig. 4 shows the putamen parcellation results in the left hemisphere of the brain for five healthy subjects with the proposed framework. The red dots denote the DMS voxels whereas the green dots represent the DLS voxels. The generated functional subROIs are spatially continuous and nicely separated.

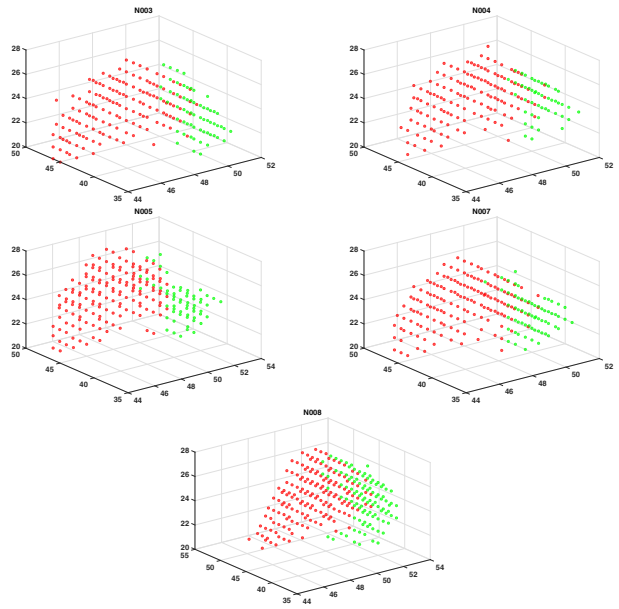

Fig. 4: Putamen subROI parcellation for five healthy subjects. The red dots denote the dorsomedial striatum (DMS) voxels and the green dots denote the dorsolateral striatum (DLS) voxels as clustered by the proposed framework.

4. CONCLUSION

In this paper, we propose a framework to define spatially continuous functional subROIs within the putamen region by exploring functional connectivities between themselves and with a few other ROIs. We generated a network that incorporates the connectivities between putamen voxels, the connectivities of other brain regions with the putamen voxels, and the spatial positions of the voxels. By applying a state of the art community detection approach on the network we were able to to sub-divide the region into several functionally connected and spatially continuous sub-regions. We evaluated the performance of the framework on synthetically generated datasets, and showed that the proposed framework outperforms other literature-based parcellation methods in terms of accuracy, specially at the presence of outliers. Although the proposed framework is applied to sub-divide a single ROI into two subROIs in putamen, this framework can be generally applied to other brain ROI for any number of functional subROI extraction.

5. REFERENCES

[1] Adriana Di Martino, Anouk Scheres, Daniel S Margulies, et al., "Functional connectivity of human striatum: a resting state fMRI study," *Cerebral cortex*, vol. 18, no. 12, pp. 2735–2747, 2008.

[2] Harrison BJ, Soriano-Mas C, Pujol J, et al., "Altered corticostriatal functional connectivity in obsessive-compulsive disorder," *Archives of General Psychiatry*, vol. 66, no. 11, pp. 1189–1200, 2009.

[3] Aaron J Gruber and Robert J McDonald, "Context, emotion, and the strategic pursuit of goals: interactions among multiple brain systems controlling motivated behavior," *Frontiers in behavioral neuroscience*, vol. 6, pp. 50, 2012.

[4] Carter T Butts, "Revisiting the foundations of network analysis," *science*, vol. 325, no. 5939, pp. 414–416, 2009.

[5] Trey Hedden and John DE Gabrieli, "Insights into the ageing mind: a view from cognitive neuroscience," *Nature reviews neuroscience*, vol. 5, no. 2, pp. 87–96, 2004.

[6] Katya Rubia, Anna B Smith, James Woolley, et al., "Progressive increase of frontostriatal brain activation from childhood to adulthood during event-related tasks of cognitive control," *Human brain mapping*, vol. 27, no. 12, pp. 973–993, 2006.

[7] Kelly Anne Barnes, Alexander L Cohen, Jonathan D Power, et al., "Identifying basal ganglia divisions in individuals using resting-state functional connectivity MRI," *Frontiers in systems neuroscience*, vol. 4, pp. 7–11, 2010.

[8] Peter Redgrave, Manuel Rodriguez, Yoland Smith, et al., "Goal-directed and habitual control in the basal ganglia: implications for Parkinson's disease," *Nature Reviews Neuroscience*, vol. 11, no. 11, pp. 760–772, 2010.

[9] Matthias Beckmann, Heidi Johansen-Berg, and Matthew FS Rushworth, "Connectivity-based parcellation of human cingulate cortex and its relation to functional specialization," *The Journal of neuroscience*, vol. 29, no. 4, pp. 1175–1190, 2009.

[10] Thorsten Kahnt, Luke J Chang, Soyoung Q Park, et al., "Connectivity-based parcellation of the human orbitofrontal cortex," *The Journal of Neuroscience*, vol. 32, no. 18, pp. 6240–6250, 2012.

[11] Richard Baumgartner, Gordon Scarth, Claudia Teichtmeister, et al., "Fuzzy clustering of gradient-echo functional MRI in the human visual cortex. Part I: Reproducibility," *Journal of Magnetic Resonance Imaging*, vol. 7, no. 6, pp. 1094–1101, 1997.

[12] Lubin Wang, Qiang Liu, Hong Li, and Dewen Hu, "Functional connectivity-based parcellation of human medial frontal cortex via maximum margin clustering," in *International Conference on Intelligent Science and Intelligent Data Engineering*. Springer, 2012, pp. 306–312.

[13] Xilin Shen, Xenophon Papademetris, and R Todd Constable, "Graph-theory based parcellation of functional subunits in the brain from resting-state fMRI data," *Neuroimage*, vol. 50, no. 3, pp. 1027–1035, 2010.

[14] Yiming Zhang, Aiping Liu, Sun Nee Tan, et al., "Connectivity-based parcellation of functional SubROIs in putamen using a sparse spatially regularized regression model," *Biomedical Signal Processing and Control*, vol. 27, pp. 174–183, 2016.

[15] Jiashun Jin, "Fast community detection by SCORE," *The Annals of Statistics*, vol. 43, no. 1, pp. 57–89, 2015.

[16] Nandinee F Haq, Sun Nee Tan, Martin J McKeown, and Z Jane Wang, "Parcellation of Functional Sub-Regions in Putamen using fMRI : A Graph Clustering Based Approach," submitted to *Biomedical Signal Processing and Control*, 2017.

[17] Jingyun Chen, Samantha J Palmer, Ali R Khan, et al., "Freesurfer-initialized large deformation diffeomorphic metric mapping with application to Parkinson's disease," in *SPIE Medical Imaging*. International Society for Optics and Photonics, 2009, pp. 725931–725931.

[18] "Freesurfer," `http://freesurfer.net/`.